GEOPHYSICAL RESEARCH LETTERS, VOL. 40, 3809–3813, doi:10.1002/grl.50709, 2013

Temporal variability of waves at the proton cyclotron frequency upstream from Mars: Implications for Mars distant hydrogen exosphere

C. Bertucci,[1,2] N. Romanelli,[1] J. Y. Chaufray,[3] D. Gomez,[1,2] C. Mazelle,[4] M. Delva,[5] R. Modolo,[3] F. González-Galindo,[6] and D. A. Brain[7]

Received 24 April 2013; revised 28 June 2013; accepted 28 June 2013; published 1 August 2013.

[1] We report on the temporal variability of the occurrence of waves at the local proton cyclotron frequency upstream from the Martian bow shock from Mars Global Surveyor observations during the first aerobraking and science phasing orbit periods. Observations at high southern latitudes during minimum-to-mean solar activity show that the wave occurrence rate is significantly higher around perihelion/southern summer solstice than around the spring and autumn equinoxes. A similar trend is observed in the hydrogen (H) exospheric density profiles over the Martian dayside and South Pole obtained from a model including UV thermospheric heating effects. In spite of the complexity in the ion pickup and plasma wave generation and evolution processes, these results support the idea that variations in the occurrence of waves could be used to study the temporal evolution of the distant Martian H corona and its coupling with the thermosphere at altitudes currently inaccessible to direct measurements. **Citation:** Bertucci, C., N. Romanelli, J. Y. Chaufray, D. Gomez, C. Mazelle, M. Delva, R. Modolo, F. González-Galindo, and D. A. Brain (2013), Temporal variability of waves at the proton cyclotron frequency upstream from Mars: Implications for Mars distant hydrogen exosphere, *Geophys. Res. Lett.*, *40*, 3809–3813, doi:10.1002/grl.50709.

1. Introduction

[2] The absence of a significant intrinsic magnetic field at Mars [*Acuña et al*., 1998] results in the direct interaction of the magnetized Solar Wind (SW) with the planet's atmosphere. Mars' interaction starts far beyond the bow shock, where exospheric particles get ionized. Ionization processes add a small amount of energy to the newborn ions with respect to their neutral precursors. As the latter are considered to be approximately at rest with respect to the planet, the planetocentric velocities of newborn ions are also assumed to be negligible. The newborn ion's initial motion in the SW frame consists in a gyration (ring component) around the interplanetary magnetic field (IMF) and a parallel motion (beam component) at the speed of its neutral precursor. The speeds of the beam and ring components are $V_{\parallel} = V_{SW}\cos(\alpha_{VB})$ and $V_{\perp} = V_{SW}\sin(\alpha_{VB})$, respectively, where α_{VB}, the IMF cone angle, is the initial pitch angle of the newborn ion and V_{SW} is the velocity of the solar wind. The newborn ion distribution function arising from the pickup of a large number of planetary ions is unstable due to the growth of plasma low frequency waves [*Wu and Davidson*, 1972]. In particular, the occurrence of waves at the local cyclotron frequency $\Omega_i = q_iB/m_i$ (B is the magnetic field strength, and q_i and m_i are the charge and mass of the ion, respectively) of a particular ion in the spacecraft (SC) frame can be associated with the occurrence of the exospheric pickup of ions with a specific mass-per-charge ratio. This represents a potentially useful diagnostic tool to detect ionized exospheric particles. An extensive discussion on the way in which magnetic field wave measurements in the SC frame can be associated with ion-ion instabilities arising from the pickup of exospheric ions can be found in *Romanelli et al.* [2013].

[3] At Mars, Phobos-2 and Mars Global Surveyor (MGS) magnetometers detected upstream waves at the local proton cyclotron frequency Ω_p [*Russell et al*., 1990, *Brain et al*., 2002; *Mazelle et al*., 2004; *Wei and Russell*, 2006; *Romanelli et al*., 2013]. All cases analyzed show a left-hand polarization in the SC frame, and a quasi-parallel propagation with respect to the IMF. *Romanelli et al*. [2013] analyzed the properties of upstream waves at Ω_p from a set of 372 MGS orbits from 27 March 1998 to 24 September 1998, during the science phasing orbits (SPO) phase. In particular, they reported a strong drop in the occurrence of waves between SPO1 (62% of the upstream observation time) and SPO2 (8%) subphases. They also noted no significant difference in the directional properties of the IMF, α_{VB}, or the IMF's convective electric field between the two subphases, suggesting that the reduction in wave occurrence could be due to temporal changes in the density of pickup protons.

[4] Theoretical and observational studies have confirmed that the source of the pickup ions responsible for the occurrence of waves at Ω_p at Mars is its hydrogen (H) exosphere via ionization processes such as photoionization and charge exchange [*Barabash and Lundin*, 2006; *Dennerl et al*., 2006]. As in the case of Venus, the Martian (H) corona has been hypothesized to contain a hot and a relatively cooler thermal population [see, e.g., *Johnson et al*., 2008]. A recent work by *Chaufray et al*. [2008] based on Mars Express SPICAM observations suggests the presence of hot

[1]Instituto de Astronomía y Física del Espacio, CONICET/UBA, Buenos Aires, Argentina.
[2]Departamento de Física, FCEN, Universidad de Buenos Aires, Buenos Aires, Argentina.
[3]LATMOS, Guyancourt, France.
[4]IRAP, Toulouse, France.
[5]IWF-ÖAW, Graz, Austria.
[6]Instituto de Astrofísica de Andalucía, Granada, Spain.
[7]Department of Astrophysical and Planetary Sciences, University of Colorado Boulder, Boulder, Colorado, USA.

Corresponding author: C. Bertucci, Institute for Astronomy and Space Physics—IAFE, Ciudad Universitaria, Buenos Aires, 1428, Argentina. (cbertucci@iafe.uba.ar)

0094-8276/13/10.1002/grl.50709

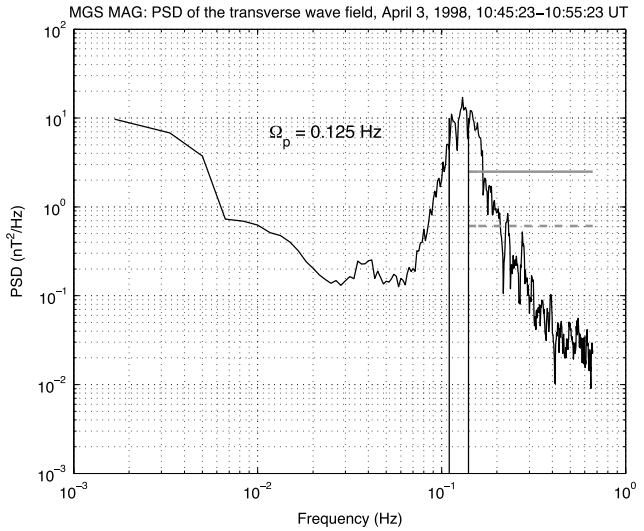

Figure 1. PSD of $\delta\mathbf{B}_\perp$ for 10:45:23–10:55:23 on 3 April 1998 for a case of positive detection of waves at $\mathbf{\Omega}_p$. Black lines indicate the frequency range corresponding to the error in the estimate of $\mathbf{\Omega}_p$ due to spacecraft fields [*Acuña et al*., 2001]. The average power density for frequencies higher than the upper limit of the interval is indicated in gray dashed lines. The gray solid line shows the average plus the STD. The latter value is 3.92 times smaller than the power in the interval around $\mathbf{\Omega}_p$.

(T > 500 K) and cold (T ~ 200 K) populations. However, the inferred hot H densities are not supported by theory, and the two-population model is still poorly constrained by observations and model errors. Other works find inconclusive evidence for a two-population model [*Feldman et al*., 2011] and provide single profiles.

[5] So far, only models and indirect observations can predict the structure of the exosphere at altitudes higher than a few scale heights above the exobase. Most models use a *Chamberlain* [1963] approach based on isothermal equilibrium. The vertical profile of the exospheric number density is an exponential whose scale height is a function of the exobase temperature and density, provided by models or observations. Long-term (timescales larger than diurnal) variations in the modeled exospheric densities come mainly from UV heating of the thermosphere. As a result, solar cycle, annual, and seasonal influences are expected. Simulations including a self-consistent calculation of the global ion production [*Modolo et al*., 2005] show that H escape is strongly dependent on the EUV flux through its influence on exospheric densities.

[6] In this work, we investigate the conditions influencing the presence or absence of upstream waves at $\mathbf{\Omega}_p$ at Mars reported in previous works [*Brain et al*., 2002, *Romanelli et al*., 2013]. We analyze MGS Magnetometer (MAG) observations during the first aerobraking (AB1) and SPO phases, and we propose an explanation based on the behavior of Mars distant H exosphere with the support of an advanced exospheric model. Then, we discuss the implications of these results in the understanding of Mars H corona and its interaction with the solar wind.

2. Observations

[7] MGS MAG is a dual fluxgate magnetometer that provides fast (up to 32 Hz), wide-range (±4, ±65,335 nT) magnetic field measurements with an uncertainty of ±1 nT due to spacecraft fields [*Acuña et al*., 2001]. Typical values for the proton cyclotron frequency at Mars' orbit (~ 0.05 Hz) justify the use of low-resolution MAG data (0.167–1.33 Hz) for which additional calibration is available.

[8] After Mars orbit insertion/capture (MOI) on 11 September 11 1998, MGS was placed in highly elliptical orbits with apoapses approximately located over the planet's South Pole. The evolution of MGS orbital period from MOI through the entire premapping phase is described in Figure 6 from *Albee et al*. [2001]. The aerobraking between MOI and April 1998 reduced the orbital period from 48 to 12 h; this phase is known as AB1. SPO came in after AB1 and ended in November 1998, when a second aerobraking (AB2) phase began. SPO orbits were 12 h long, and local times monotonically varied between noon and 4 AM. During AB1 and SPO, the southern latitudes of the apoapses remained high.

[9] The upstream segments of every AB1 and SPO orbit up to an altitude of 20,400 km (6 R_M) were examined in the search for waves at $\mathbf{\Omega}_p$. The upper altitude limit was chosen so as to ensure a homogeneous altitude coverage throughout AB1 and SPO. Since these waves propagate almost parallel to the IMF [*Romanelli et al*., 2013], the criterion used to identify them was based on the Fourier power spectral density (PSD) of the transverse wave components with respect to the IMF ($\delta\mathbf{B}_\perp$). The PSD of $\delta\mathbf{B}_\perp$ is the norm of a vector whose components are the power spectral densities of the components of $\delta\mathbf{B}_\perp$. The PSD is estimated over sliding 10 min intervals to ensure a large number of wave periods while allowing changes in the IMF. Consecutive intervals have an overlap of 1 min. Upstream portions are identified using the points where MGS trajectory crosses *Vignes et al*. [2000] bow shock fit, assuming an error of 10 min on the upstream side along the spacecraft trajectory.

[10] We define that waves at $\mathbf{\Omega}_p$ are detected when the average PSD within the frequency band $\mathbf{\Omega}_p \pm 0.015$ Hz (0.015 Hz being the error in $\mathbf{\Omega}_p$ associated with MAG's uncertainty) is larger than the average PSD for frequencies $\omega > \mathbf{\Omega}_p + 0.015$ Hz, plus its standard deviation (STD), multiplied by a constant $k > 1$. If f_N is the Nyquist frequency (0.167 and 0.667 Hz for the two low frequency waves sampling rates available), this is

$$\langle PSD(\omega)\rangle_{\Omega-0.015Hz}^{\Omega p+0.015Hz} > k\left\{\langle PSD(\omega)\rangle_{\Omega p+0.015Hz}^{f_N} + STD\{PSD(\omega)\}_{\Omega p+0.015Hz}^{f_N}\right\}$$

[11] The value of k is obtained by inspecting several orbits with and without a clear spectral line at $\mathbf{\Omega}_p$. A value of k = 2.5 was found to be acceptable, as all selected orbits show signatures at $\mathbf{\Omega}_p$, and their number is adequate for statistical purposes. Similar criteria have been applied on Venus Express magnetometer measurements [*Delva et al*., 2011, and references therein].

[12] Figure 1 shows an example of a positive detection of waves at $\mathbf{\Omega}_p$. The plot shows the PSD of $\delta\mathbf{B}_\perp$ as a function of frequency ω for the interval 10:45:23–10:55:23 on 3April 1998. The spectrum shows a peak at $\mathbf{\Omega}_p = 0.125$ Hz in the SC frame. The power contained in the 0.105–0.135 Hz band (black lines) is higher than the average power contained at higher frequencies (gray dash line), plus its STD (gray solid line).

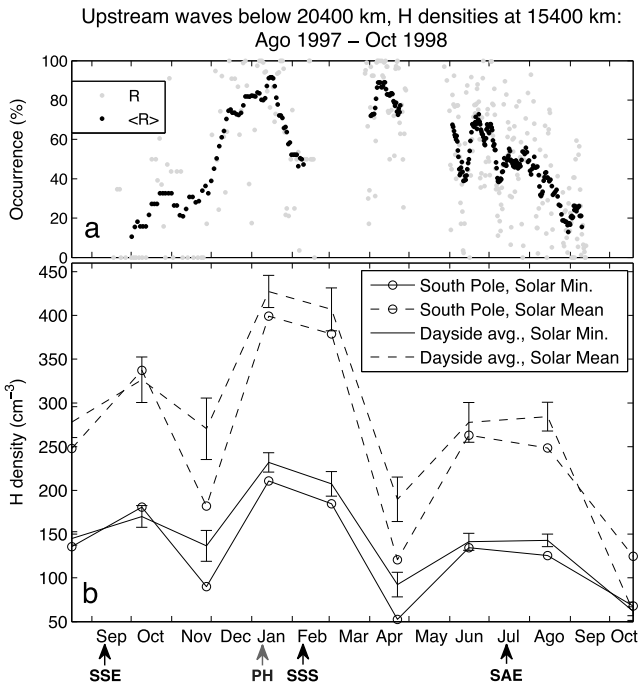

Figure 2. (a) Occurrence of upstream waves at Ω_p below 20,400 km altitude from September 1997 through September 1998. Rates per orbit (R, gray dots) and 15-orbit averaged (<R>, black dots) are displayed. (b) Modeled H density above Mars South Pole and dayside-averaged H density at 15,400 km altitude for minimum and mean solar activity from August 1997 to October 1998. Mars perihelion (PH, 7 January 1998), southern hemisphere spring equinox (SSE, 12 September 1997), southern hemisphere summer solstice (SSS, 6 February 1998), and southern hemisphere autumn equinox (SAE, 14 July 1998) are indicated.

[13] An upstream wave occurrence rate R was defined for each orbit as the number of intervals meeting the criterion above, divided by the total number of intervals. To investigate the long-term (seasonal and annual) variability, R was averaged every 15 orbits with a 14-orbit overlap. The averaged occurrence rate was called <R>.

3. Results and Discussion

[14] Figure 2a shows the value of R and <R> between 14 September 1997 and 17 September 1998. Data gaps correspond to the AB1-SPO1 transition (20 February–26 March 1998), and solar conjunction hiatus (30 April–26 May 1998). In what follows, we describe the behavior of <R> in order to understand the long-term variability of the wave occurrence. Soon after MOI—around the southern spring equinox (12 September 1997)—<R> increases until a local maximum of 32% in late October 1997. After a brief decline in the occurrence to ~21% in early November 1997, <R> undergoes a strong increase, which ends around Mars perihelion (7 January 1998), where waves are observed in 92% of the time. After 12 January, the wave abundance drops until it hits the first data gap. During the entire SPO1 (April 1998), high values of <R> (around 80%) are observed. After solar conjunction, a more gradual decrease is observed in SPO2, with values around 20% during early southern autumn. In spite of the altitude restriction used in this study, occurrence rates are consistent with estimates obtained by *Brain et al*. [2002].

[15] Figure 2a suggests a temporal dependence in the abundance of upstream waves at Ω_p. The hypothesis that any variability in the wave occurrence at a given location is attributed to temporal effects is supported by the strong difference in wave abundance for orbits with similar geometry, and the absence of a manifest influence upon the convective electric field or the IMF direction [*Romanelli et al*., 2013]. In what follows, changes in the efficiency of the wave generation mechanism, the properties of the solar wind, the efficiency of the ionization mechanisms, and/or the local exospheric H density are discussed in the context of MGS observations.

3.1. Wave Generation and Evolution

[16] A central question is how representative the presence of waves at Ω_p is for the local neutral density. *Cowee et al*. [2012] suggest that the increase in the amplitude of waves at Ω_p is due to the increase in the local pickup ion density and the cumulative ion production upstream of the observation point. As exospheric densities increase, increases in both the local and cumulative ion productions are expected. Accordingly, higher occurrence rates will be expected at Ω_p as long as nonlinear effects do not degrade the wave spectra below the detection threshold. According to *Cowee et al*., [2012], the observed waves would be below nonlinear saturation.

[17] Also the wavelength for maximum linear growth rates at least for the ion-ion right-hand mode is on the order of a Martian radius [*Bertucci et al*., 2005], setting a limit on the spatial resolution in the use of waves as indicators of exospheric densities.

3.2. Changes in Solar Wind Parameters and Ionization Rates

[18] Self-consistent hybrid simulations [*Modolo et al*., 2005] suggest that charge exchange is the main source of escaping protons and that the escape rate of these protons is four times higher during solar minimum with respect to solar maximum due to the expansion of the neutral H corona. Although MGS measurements are not able to characterize the photoionization and charge exchange rates, the solar activity during the premapping phase was typical of a minimum, suggesting that both ionization rates would not have experienced major alterations. In agreement with this view, recent works addressing the generation of the same type of waves [*Cowee et al*., 2012] assume constant ionization rates.

[19] Transient solar wind disturbances such as Interplanetary Coronal Mass Ejections (ICMEs) have been proven to alter significantly the Martian plasma environment [*Crider et al*., 2005]. However, the low solar activity, the absence of drastic short-term (a few days long) changes in <R>, and the fact that from September 1997 to September 1998 the solar F10.7 flux at Mars did not vary significantly ($107.90 \pm 18.59\,\mathrm{cm^{-2}\,s^{-1}}$) all suggest that such events might not be the cause of the long-term variability observed in the averaged wave occurrence.

3.3. Changes in the Extent of the Distant Martian Hydrogen Corona

[20] Figure 2b shows the H exospheric density at 15,400 km altitude above the Martian South Pole and the density averaged over the entire dayside hemisphere at the

same altitude, between August 1997 and October 1998. H densities for minimum and mean solar activity conditions are provided by a 3D exospheric model [*Chaufray et al*. 2012], which incorporates nonuniform densities and temperatures at the exobase from a 3D Laboratoire de Météorologie Dynamique Global Climate Model (LMD-GCM) model [*González-Galindo et al*., 2009]. Values initially given as a function of solar longitude are then converted to time using MGS ephemeris. The 15,400 km altitude level was chosen based on the average altitude of MGS for the chosen data set. Two basic properties are immediately evident. First, H densities increase with solar activity, which reveals the UV control of the thermosphere. Second, the influence of solar declination and heliocentric distance is manifested in density curves displaying annual maxima around Mars perihelion and southern summer solstice (6 February 1998) and lower values during spring and autumn. Third, H densities are not symmetric around their maxima. This is probably due to heliocentric distance effects (aphelia occurred on 29 January 1997 and 16 December 1998, respectively). In addition to this trend, the model predicts oscillations in density in timescales of a few months. The amplitude of these oscillations is smaller for the dayside profiles, probably indicating a seasonal effect. In spite of these differences, however, the dayside average and South Pole density curves display maxima at perihelion.

[21] Although the wave growth rate depends on several factors, the observed variability in $<R>$ could be related with the annual and seasonal changes in the H profile predicted by our exospheric model. First, the average wave occurrence and the H density curves show maxima around perihelion/southern summer solstice and display lower values around the equinoxes, suggesting that the occurrence of waves could be influenced by the expansion or contraction of the planet's exosphere in response to annual/seasonal changes in solar UV heating. Second, wave occurrence and density curves display oscillations in timescales on the order of a few months. However, the timescales of the density oscillations predicted by the exospheric model seem to be longer, degrading any possible correlation. Third, densities for the South Pole and dayside show similar behaviors suggesting that at those altitudes, H density and ultimately wave occurrence could be more sensitive to annual rather than seasonal changes. Finally, the influence of a possible change in solar activity remains elusive. In principle, the low variability in the F10.7 flux suggests that MGS measurements might have taken place during solar minimum conditions.

[22] This comparison provides a possible explanation to the temporal variability in the occurrence of waves at Ω_p based on the expansion and contraction of the Martian H exosphere due to annual and seasonal components in the solar UV heating of the thermosphere. If this is confirmed, the temporal variability in the occurrence of waves at Ω_p could be used to study the coupling of the thermosphere with the exosphere of Mars [*Bougher et al*., 1999], where direct observations are unavailable. In particular, wave observations coincide with the occurrence of dust storms [*Keating et al*., 1998; *Clancy et al*., 2000] with known effects on the Martian thermosphere.

[23] The influence of the exosphere in the Martian solar wind interaction has also been suggested to be responsible for other plasma structures such as the magnetic pileup boundary [MPB; see, e.g., *Crider et al*., 2000]. *Brain et al*., [2005] revealed that the altitude of the northern MPB (i.e., far from the influence of crustal fields) is sensitive to Martian seasons. The question whether or not this behavior is related to the hypotheses presented here is beyond the scope of this work. Nevertheless, all these results suggest that in addition to the solar cycle, the annual and seasonal variability in the UV irradiance could be a potentially important component of the temporal evolution of the Martian plasma environment.

4. Conclusions

[24] The pickup of exospheric ions, and the subsequent growth and evolution of plasma waves via microscopic plasma interactions are complex physical processes. By virtue of a particular property of waves propagating along the IMF and originating from exospheric ion pickup, the analysis of the occurrence of upstream transverse fluctuations at Ω_p at high southern latitudes shows that the abundance of such waves varies with time. This variability is found to display a similar long-term trend as those of the densities of exospheric H obtained from models, which take the effect of thermospheric heating by solar UV radiation into account. The underlying assumption is that wave generation mainly depends on the H density and that ionization rates remain constant. This approach follows previous works, which suggest that the increase in the ion production is due to changes in the exospheric densities.

[25] Future studies will focus on the relation between exospheric densities and the amplitudes of upstream waves. This will require the support of numerical simulations including linear and nonlinear wave evolution where ion pickup rates display a spatial gradient. Also, the use of improved exospheric models and more comprehensive measurements (such as those to be carried out by the MAVEN mission) will help to confirm or disprove the proposed interpretation. In particular, the effects of the vertical transfer of energy and momentum at different timescales, including the role of global dust storms should be investigated.

[26] **Acknowledgments.** Authors thank the International Space Science Institute and the ECOS/MINCYT and BMWF/MINCYT programs. F.G.G. is funded by a CSIC JAE-Doc contract cofinanced by the European Social Fund.

[27] The Editor thanks Jared Espley and an anonymous reviewer for their assistance in evaluating this paper.

References

Acuña, M., et al. (1998), Magnetic field and plasma observations at Mars: Initial results of the Mars Global Surveyor Mission, *Science*, *279*, 1676–1680.

Acuña, M. H., et al. (2001), Magnetic field of Mars: Summary of results from the aerobraking and mapping orbits, *J. Geophys. Res.*, *106*(E10), 23,403–23,418.

Albee, A. L., et al. (2001), Overview of the Mars Global Surveyor mission, *J. Geophys. Res.*, *106*(E10), 23,291–23,316, doi:10.1029/2000JE001306.

Barabash, S., and R. Lundin (2006), ASPERA-3 on Mars Express, *Icarus*, *182*(2), 301–307.

Bertucci, C., C. Mazelle, and M. Acuña (2005), Interaction of the solar wind with Mars from Mars Global Surveyor MAG/ER observations, *J. Atmos. Sol. Terr. Phys.*, *67*, 1797–1808, doi:10.1016/j.jastp.2005.04.007.

Bougher, S., et al. (1999), Mars Global Surveyor aerobraking: atmospheric trends and model interpretation, *Adv. Space Res.*, *23*(11), 1887–1897.

Brain, D. A., et al. (2002), Observations of low frequency electromagnetic plasma waves upstream from the Martian shock, *J. Geophys. Res.*, *107*(A6), 1076, doi:10.1029/2000JA000416.

Brain, D. A., et al. (2005), Variability of the altitude of the Martian sheath, *Geophys. Res. Lett.*, *32*, L18203, doi:10.1029/2005GL023126.

Chamberlain, J. W. (1963), Planetary coronae and atmospheric evaporation, *Planet. Space Sci.*, *11*(8), 901–960.

Chaufray, J. Y., et al. (2008), Observation of the hydrogen corona with SPICAM on Mars Express, *Icarus*, *195*(2), 598–613.

Chaufray J.-Y., et al. (2012), Current status on Mars exospheric studies, 39th COSPAR Scientific Assembly, Mysore: India - hal-00740343.

Clancy, R. T., et al. (2000), An intercomparison of ground-based milimeter, MGS TES, and Viking atmospheric temperature measurements: Seasonal and interannual variability of temperatures and dust loading in the global Mars atmosphere, *J. Geophys. Res.*, *105*(E4), 9553–9571.

Cowee, M. M., et al. (2012), Pickup ions and ion cyclotron wave amplitudes upstream of Mars: first results from the 1D hybrid simulation. *Geophys. Res. Lett.*, *39*, L08104, doi:10.1029/2012GL051313.

Crider, D. H., et al. (2000), Evidence of electron impact ionization in the magnetic pileup boundary of Mars, *Geophys. Res. Lett.*, *27*(1), 45–48.

Crider, D. H., et al. (2005), Mars Global Surveyor observations of the Halloween 2003 solar superstorm's encounter with Mars, *J. Geophys. Res.*, *110*, A09S21, doi:10.1029/2004JA010881.

Delva, M., et al. (2011), Upstream Ion Cyclotron Waves at Venus and Mars, *Space Sci. Rev.*, *162*(1–4), 5–24.

Dennerl, K., et al. (2006), First observation of Mars with XMM–Newton. High resolution X-ray spectroscopy with RGS, *Astron. Astrophys.*, *451*, 709–722.

Feldman, P., et al. (2011), Rosetta-Alice observations of exospheric hydrogen and oxygen on Mars, *Icarus*, *214*(2), 394–399.

González-Galindo, F., et al. (2009), A ground-to-exosphere Martian circulation model: 1. Seasonal, diurnal, and solar cycle variation of thermospheric temperatures, *J. Geophys. Res.*, *114*, E04001, doi:10.1029/2008JE003246.

Johnson, R. E., et al. (2008), Exospheres and Atmospheric Escape, *Space Sci. Rev.*, *139*, 355–397, doi:10.1007/s11214-008-9415-3.

Keating, G. M., et al. (1998), The Structure of the Upper Atmosphere of Mars: In Situ Accelerometer Measurements from Mars Global Surveyor, *Science*, *279*(5357), 1672–1676.

Mazelle, C., et al. (2004), Bow shock and upstream phenomena at Mars, *Space Sci. Rev.*, *111*, 115–181.

Modolo, R., et al. (2005), Influence of the solar EUV flux on the Martian plasma environment, *Ann. Geophys.*, *23*(2), 433–444.

Romanelli, N., et al. (2013), Proton cyclotron waves upstream from Mars: Observations from Mars Global Surveyor, *Planet. Space Sci.*, *76*, 1–9.

Russell, C. T., et al. (1990), Upstream waves at Mars—PHOBOS observations, *Geophys. Res. Lett.*, *17*(6), 897–900.

Vignes, D., et al. (2000), The Solar Wind interaction with Mars: locations and shapes of the Bow Shock and the Magnetic Pile-up Boundary from the observations of the MAG/ER experiment onboard Mars Global Surveyor, *Geophys. Res. Lett.*, *27*(1), 49–52.

Wei, H., and Russell, C. T. (2006), Proton cyclotron waves at Mars: exosphere structure and evidence for a fast neutral disk, *J. Geophys. Res.*, *33*, L23103, doi:10.1029/2006GL026244.

Wu, C. S., and R. C. Davidson (1972), Electromagnetic instabilities produced by neutral-particle ionization in interplanetary space, *J. Geophys. Res.*, *77*(28), 5399.